THE JOURNAL OF PHYSICAL CHEMISTRY C

Article

pubs.acs.org/JPCC

Flexible Hybrid Membranes of $NiCo_2O_4$-Doped Carbon Nanofiber@MnO_2 Core–Sheath Nanostructures for High-Performance Supercapacitors

Feili Lai,[†] Yue-E Miao,[†] Yunpeng Huang,[†] Tai-Shung Chung,[‡] and Tianxi Liu*,[†]

[†]State Key Laboratory of Molecular Engineering of Polymers, Department of Macromolecular Science, Fudan University, Shanghai 200433, PR China

[‡]Department of Chemical & Biomolecular Engineering, National University of Singapore, 4 Engineering Drive 4, Singapore 117576, Singapore

Supporting Information

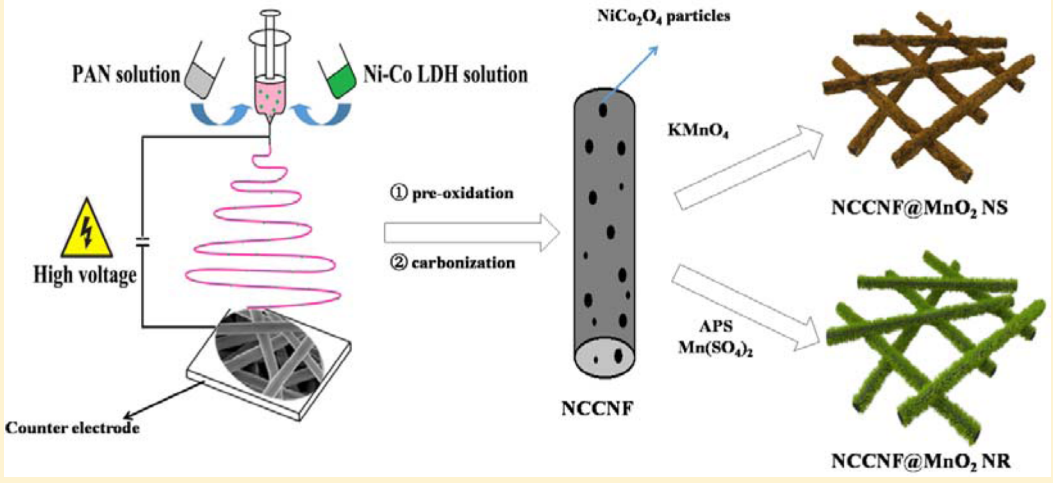

ABSTRACT: Construction of MnO_2-based hybrid nanostructures with carbonaceous materials has been considered as one of the most efficient strategies to overcome excessive aggregations of MnO_2 particles. Here, a facile approach of growing δ-phase and γ-phase MnO_2 with distinctly different morphologies on highly conductive $NiCo_2O_4$-doped carbon nanofibers (NCCNFs) through the combination of electrospinning, solution codeposition, and redox deposition methods is presented to form NCCNF@MnO_2 nanosheet (or nanorod) core–sheath nanostructures. The obtained two kinds of flexible hybrid membranes with hierarchical nanostructures are both evaluated as electrodes for high-performance supercapacitors. The greatly improved specific surface areas for ionic adsorption, significantly enhanced conductivity of NCCNF, and an open three-dimensional network for rapid electron transportation during the electrochemical processes jointly lead to remarkably enhanced specific capacitances of 918 and 827 F g^{-1} (based on the active materials) at a scan rate of 2 mV s^{-1} and good cycling ability with 83.3% and 87.6% retention after 2000 cycles for NCCNF@MnO_2 nanosheet and NCCNF@MnO_2 nanorod hybrid membranes, respectively. Therefore, this work suggests a novel strategy for design and potential application of MnO_2 hybrid materials in high-performance supercapacitors.

1. INTRODUCTION

Supercapacitors, also called electrochemical capacitors (ECs), have attracted great attention due to their numerous desirable properties, such as fast charge/discharge process, long-term stability, and high power density.[1−6] Countless materials have been widely investigated as electrode materials for ECs, including carbonaceous materials, conducting polymers, and metal oxides/hydroxides.[7−9] Among the metal oxides/hydroxides (e.g., RuO_2, MnO_2, Co_3O_4, $Ni(OH)_2$), MnO_2 is one of the most attractive materials because of its low cost, environmental compatibility, and high theoretical pseudocapacitance.[10−14] Subramanian et al. have synthesized various manganese oxide nanostructures with capacitance values in the range of 72−168 F g^{-1} by controlling the synthesis conditions.[15] However, due to their intrinsically poor electrical conductivity and severe aggregation during the electrochemical process, conventional MnO_2 electrode materials show low capacitances ranging from 150 to 300 F g^{-1}, which are far less than the theoretical value of

Received: March 21, 2015
Revised: May 20, 2015
Published: May 27, 2015

DOI: 10.1021/acs.jpcc.5b02739
J. Phys. Chem. C 2015, 119, 13442−13450

1370 F g^{-1}.[16−19] Therefore, it is essential to improve the conductivity and dispersion of MnO_2 nanoparticles to approach its theoretical capacitance.

An effective strategy has been exploited by developing MnO_2/carbonaceous hybrid materials, such as MnO_2/carbon nanofoam, MnO_2/carbon nanotubes, MnO_2/graphene, MnO_2/carbon nanofibers, and MnO_2/carbon aerogel hybrid materials, to efficiently improve their electrochemical performance.[20−25] You et al. reported a ternary nanocomposite of MnO_2, carbon nanotubes, and graphene oxide as electrode material, showing ideal capacitive behavior, large specific capacitance, high energy density, and power density.[26] Zhao et al. developed a facile preparation of powdery carbon@MnO_2 core−shell hybrid nanospheres with various nanostructures of MnO_2 shells by simply controlling the reaction time. The hybrid nanospheres thus obtained exhibit a high capacitance of 252 F g^{-1} (based on the mass of MnO_2) at a scan rate of 2 mV s^{-1} and good cycling ability with 74% retention after 2000 cycles.[27] In spite of the excellent electrochemical performance, most of the above powdery materials need to be blended with conductive and binding agents to form film electrodes. Nevertheless, the poor mechanical properties of thus mixed electrode materials dramatically restrict their practical application as high-performance electrodes for supercapacitors. Worse still, introduction of excess binding agents severely affects the conductivity and electrochemical performance of film electrodes. Therefore, it is of significance to develop binder-free electrode materials to meet the ever-increasing demands in flexible and portable electronic equipment.[28]

Electrospinning has been considered as an effective approach to produce continuous fiber membranes as a binder-free carbonaceous template, which exhibits micron-sized or even nanosized fiber diameter, large specific surface area and excellent mechanical properties.[29−31] Beneficial from these outstanding characteristics, electrospun carbon nanofiber (CNF) membranes are promising as electrode materials for Li-ion batteries, supercapacitors, and electrochemical catalysis.[31−34] Additionally, the conductivity of electrospun CNF can be dramatically increased by incorporating conductive polymers or metal oxides, which will be beneficial to maintain high specific capacitances even at high scan rates.[35,36] Nickel−cobalt oxide ($NiCo_2O_4$) is one kind of highly conductive binary metal oxide, which can dramatically enhance the electrochemical performance of the carbonaceous template due to its inherently pseudocapacitive characteristics. Therefore, it is a strategic way to hybridize $NiCo_2O_4$ into electrospun carbon nanofibers as high-performance membrane electrodes for next-generation energy storage devices.

In this work, $NiCo_2O_4$-doped carbon nanofiber@MnO_2 nanosheet (NS) and nanorod (NR) hybrid membranes are facilely fabricated through the combination of electrospinning, solution codeposition, and redox deposition methods. By constructing $NiCo_2O_4$-doped carbon nanofibers (NCCNFs) with two-dimensional (2D) MnO_2 nanosheets or one-dimensional (1D) MnO_2 nanorods, novel core−sheath nanostructures of the NCCNF@MnO_2 nanosheet and NCCNF@MnO_2 nanorod are generated to efficiently prevent the aggregation of MnO_2 nanoparticles, increase the specific surface area, and offer an open three-dimensional (3D) network for rapid electron transport during the charge−discharge processes. Typically, remarkably enhanced capacitive performance is achieved with the specific capacitance of 918 and 827 F g^{-1} (based on the active materials) at a scan rate of 2 mV s^{-1} for the NCCNF@MnO_2 nanosheet and NCCNF@MnO_2 nanorod hybrid membranes, respectively. Furthermore, this facile and universal method can be extended to the fabrication of other hierarchically organized hybrid membranes combining carbonaceous and pseudocapacitive materials for potential high-performance supercapacitor applications.

2. EXPERIMENTAL SECTION

2.1. Materials. Polyacrylonitrile (PAN, Mw = 150 000 g mol^{-1}) was purchased from Sigma-Aldrich. Nickel nitrate hexahydrate ($Ni(NO_3)_2·6H_2O$) was purchased from Aladdin Chemical Reagent Co. Cobalt nitrate hexahydrate ($Co(NO_3)_2·6H_2O$), hexamethylenetetramine (HMT), potassium permanganate ($KMnO_4$), manganese sulfate monohydrate ($MnSO_4·H_2O$), ammonium persulfate ($(NH_4)_2S_2O_8$, APS), *N*,*N*-dimethylformamide (DMF), sodium hydroxide (NaOH), and sulfuric acid (H_2SO_4) were all purchased from Sinopharm Chemical Reagent Co. All chemicals were of analytic grade and used without further purification.

2.2. Preparation of Electrospun NCCNF@MnO_2 NS and NR Hybrid Membranes. First, powdery Ni−Co layered double hydroxides (Ni−Co LDH) were synthesized by the solution codeposition method. Briefly, 0.5 mmol of $Ni(NO_3)_2·6H_2O$, 1.0 mmol of $Co(NO_3)_2·6H_2O$, and 5 mmol of HMT were dissolved in a mixed solvent of 20 mL of ethanol and 20 mL of deionized water to form a transparent pink solution. The mixed solution was kept in an oil bath at 80 °C for 8 h to achieve light green precipitates of Ni−Co LDH, which was then washed with deionized water and ethanol, isolated by centrifugation, and dried at 70 °C for 24 h.

Second, 200 mg of dried Ni−Co LDH powder was dissolved in 5 mL of DMF to form Ni−Co LDH solution, and 1.0 g of PAN powder was dissolved in 5 mL of DMF under magnetic stirring for 6 h to form PAN solution. Then, these two solutions were mixed together under magnetic stirring for another 6 h to form a transparent bicomponent spinning solution, which was sucked into a 10 mL plastic syringe with a stainless steel needle having an inner diameter of 0.5 mm. The electrospun membranes were produced at an applied voltage of 18 kV with a feeding speed of 1 mL h^{-1} and a distance of 15 cm between the needle tip and aluminum foil collector. After collecting for 45 min, electrospun Ni−Co LDH-doped PAN hybrid membranes were generated. The obtained membranes were then preoxidized to 250 °C in air atmosphere for 2 h with a heating rate of 2 °C min^{-1}, followed by heating up to 600 °C in a nitrogen flow with a heating rate of 3 °C min^{-1} and holding there for half an hour. Thus, with PAN nanofibers turning into carbon nanofibers and Ni−Co LDH dehydrating to form $NiCo_2O_4$ particles, $NiCo_2O_4$-doped carbon nanofiber (NCCNF) membranes were obtained.

Finally, the NCCNF membranes were immersed into a purple-red solution of $KMnO_4$ at 80 °C in an oil bath for 10 h. After the redox deposition reaction, the synthesized hybrid membranes were rinsed with deionized water several times and dried in a vacuum oven at 60 °C for 6 h. According to different weight ratios of NCCNF membranes to $KMnO_4$ (varying from 5:1, 2:1, 1:1, 1:2, to 1:5), the samples prepared by the above-mentioned steps were, respectively, labeled as NCCNF@MnO_2 NS-1, NCCNF@MnO_2 NS-2, NCCNF@MnO_2 NS-3, NCCNF@MnO_2 NS-4, and NCCNF@MnO_2 NS-5. Meanwhile, bare carbon nanofiber membranes coated with MnO_2 nanosheets (denoted as CNF@MnO_2 NS-1:1) were also synthesized in the same way with equal weight proportion of

DOI: 10.1021/acs.jpcc.5b02739
J. Phys. Chem. C 2015, 119, 13442−13450

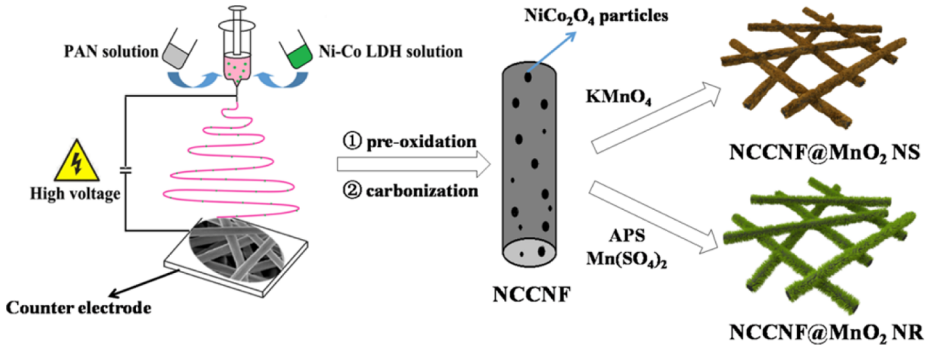

Figure 1. Schematic illustration for the preparation of NCCNF@MnO_2 NS and NR hybrid membranes.

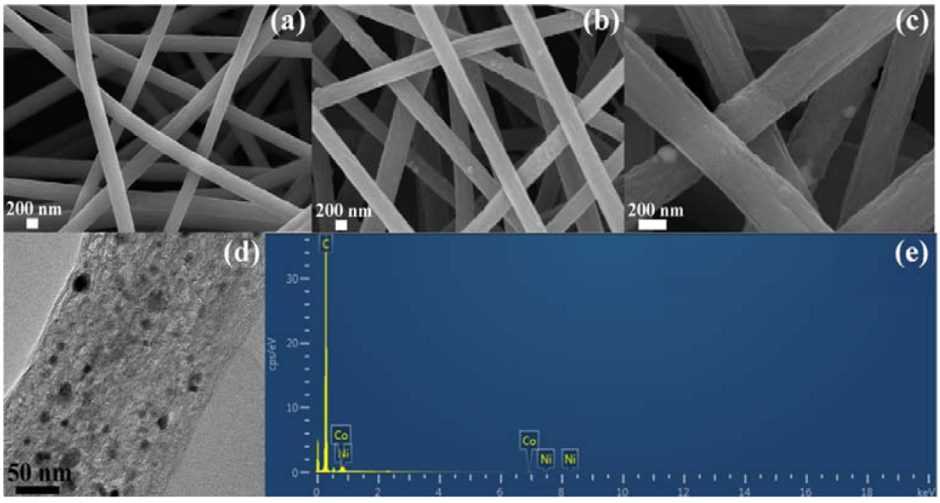

Figure 2. FESEM images of (a) the bare electrospun CNF membrane, (b) Ni−Co LDH-doped PAN hybrid membrane, (c) $NiCo_2O_4$-doped CNF hybrid membrane, (d) TEM image of the $NiCo_2O_4$-doped CNF, and (e) the corresponding EDS spectrum of $NiCo_2O_4$-doped CNF in (c).

CNF membranes to $KMnO_4$. The redox reaction during the synthesis of MnO_2 nanosheets is given below[37]

$$4KMnO_4 + 3C + H_2O = 4MnO_2 + 2KHCO_3 + K_2CO_3 \quad (1)$$

Analogously, NCCNF membranes coated with MnO_2 nanorods (denoted as NCCNF@MnO_2 NRs) were easily prepared through the redox deposition method by replacing $KMnO_4$ solution with 40 mL of aqueous solution containing 8 mmol of $MnSO_4{\cdot}H_2O$ and 8 mmol of APS at 80 °C in an oil bath for 2 h. Simultaneously, bare carbon nanofiber membranes coated with MnO_2 nanorods (denoted as CNF@MnO_2 NR) were synthesized via the same way for comparison. The chemical reaction between Mn^{2+} and $S_2O_8^{2-}$ can be formulated by the following equation[38]

$$MnSO_4 + (NH_4)_2S_2O_8 + 2H_2O = MnO_2 + (NH_4)_2SO_4 + 2H_2SO_4 \quad (2)$$

All of the prepared membranes were washed with deionized water several times to remove byproducts on the surface of samples. The whole preparation procedures of NCCNF@MnO_2 NS and NR membranes are schematically shown in Figure 1.

2.3. Characterization. Morphologies of the samples were observed by a field emission scanning electron microscope (FESEM, Ultra 55, Zeiss) at an acceleration voltage of 5 kV. Transmission electron microscopy (TEM) was performed by a JEOL JEM 2100 TEM at an acceleration voltage of 200 kV. Phase structures of the samples were investigated by X-ray diffraction (XRD, X'pert PRO, PANalytical) with Cu Kα radiation (λ = 0.1542 nm) at an angular speed of (2θ) 5° min^{-1} from 10° to 70° under a voltage of 40 kV and a current of 40 mA. The surface chemical compositions of the samples were analyzed by X-ray photoelectron spectroscopy (XPS) on a RBD upgraded PHI-5000C ESCA system (PerkinElmer) with Al Kα ($h\nu$ = 1486.6 eV). All XPS spectra were corrected using the C 1s line at 284.6 eV, while curve fitting and background subtraction were accomplished using RBD AugerScan 3.21 software. Thermogravimetric analyses (Pyris 1 TGA) were performed under air flow from 100 to 800 °C at a heating rate of 20 °C min^{-1}. To emphasize, due to the tiny contribution of $NiCo_2O_4$ for the hybrid materials, the active materials in manuscript only refer to the MnO_2 part.

2.4. Electrochemical Measurements. Electrochemical measurements were performed in 1 M Na_2SO_4 aqueous solution on an electrochemical workstation (CHI600E, Chenhua Instruments Co. Ltd., Shanghai) with a standard three-electrode setup, where the as-obtained membrane was directly used as the working electrode and Ag/AgCl and Pt wire as the reference and counter electrode, respectively. The voltage window of cyclic voltammograms (CVs) was 0−0.8 V with different scan rates ranging from 2 to 100 mV s^{-1}. Galvanostatic charge−discharge testing was performed between 0 and 0.8 V at different current densities from 0.5 to 20 A g^{-1}. The electrochemical impedance spectroscopy (EIS) measure-

DOI: 10.1021/acs.jpcc.5b02739
J. Phys. Chem. C 2015, 119, 13442−13450

ments were conducted by applying an AC voltage in the frequency range from 10 mHz to 100 kHz with 5 mV amplitude. The specific capacitance (C) of the electrode can be calculated from CV and galvanostatic charge−discharge curves according to the following equations

$$C = \frac{\int I\mathrm{d}V}{vmV} \tag{3}$$

$$C = \frac{I \times \Delta t}{mV} \tag{4}$$

where I (A) is the current; V (V) is the potential; v (mV s^{-1}) is the potential scan rate; m (g) is the mass of the electroactive materials in the electrodes; and Δt (s) is the discharge time.

3. RESULTS AND DISCUSSION

FESEM images of bare electrospun carbon nanofibers are shown in Figure 2a. The average diameter of CNF is about 300 nm with a smooth surface and uniform diameter distribution. Figure 2b shows the morphology of Ni−Co LDH-doped PAN nanofibers with embossed Ni−Co LDH nanoparticles on the surface. After heat treatment for preoxidation and carbonization, $NiCo_2O_4$-doped carbon nanofibers (NCCNF) were obtained as shown in Figure 2c, which shows morphology similar to Ni−Co LDH-doped PAN nanofibers except with a slight decrease in fiber diameter due to the pyrogenic decomposition and cyclization reaction of PAN chains. The morphology of NCCNF thus formed is further investigated by TEM (Figure 2d). Uniformly distributed $NiCo_2O_4$ nanoparticles with a size range from 10 to 20 nm can be clearly observed inside carbon nanofibers, indicating a homogeneous internal doping of $NiCo_2O_4$ nanoparticles. The energy-dispersive spectrum (EDS) for the selected area of NCCNF is presented in Figure 2e with obvious energy peaks of Ni and Co elements, which gives further evidence for the successful hybridization of $NiCo_2O_4$ particles inside CNF. The existence of $NiCo_2O_4$ nanoparticles in CNF can not only increase the electrical conductivity of bare carbon nanofiber membranes but also act as energy storage units to enhance their electrochemical performance. Additionally, the rough surface induced by $NiCo_2O_4$ nanoparticle incorporation produces more active sites for the subsequent growth of MnO_2 nanosheets and nanorods.

Via the redox deposition method, MnO_2 nanosheets are uniformly anchored on the surface of $NiCo_2O_4$-doped CNF to form a core−sheath structure of the NCCNF@MnO_2 nanosheet. As shown in Figure 3a, MnO_2 nanosheets are thin and sparsely distributed on the surface of NCCNF, due to the limited manganese sources. With the increase of weight ratio of NCCNF membrane to $KMnO_4$, NCCNFs are gradually covered with thickly and densely distributed MnO_2 nanosheets, resulting in ever-increasing fiber diameters (Figure 3b−d). When the weight ratio of the NCCNF membrane to $KMnO_4$ is 1:5, a 2-fold increase in the fiber diameter to about 600 nm (Figure 3e) can be observed, compared with the diameter of NCCNF (Figure 2c). Figure 3f shows the digital photo of the highly flexible NCCNF@MnO_2 nanosheet hybrid membrane, which can be directly used as electrode material without the cumbersome process of preparing a composite of conductive additives and polymer binders as reported previously.[39] Meanwhile, the uniform growth of 2D MnO_2 nanosheets on intersecting 1D carbon nanofibers with $NiCo_2O_4$ doping can

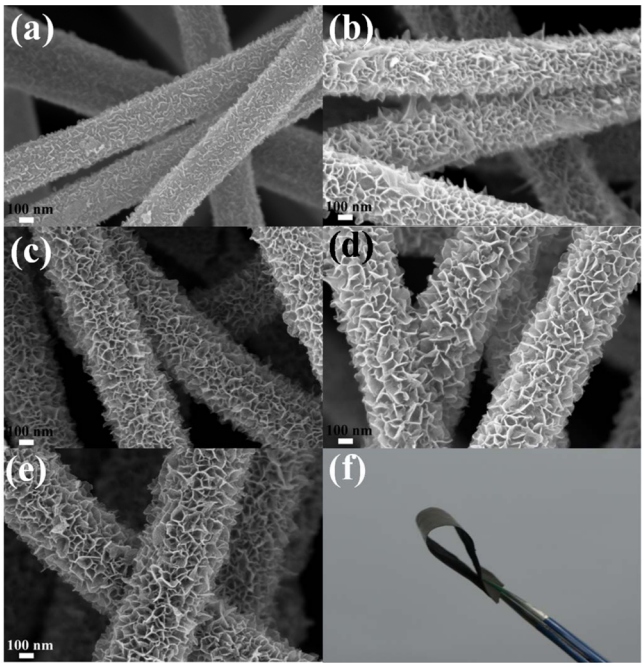

Figure 3. FESEM images of NCCNF@MnO_2 NS with different weight ratios of NCCNF membrane to $KMnO_4$ (varying from 5:1, 2:1, 1:1, 1:2, to 1:5): (a) NCCNF@MnO_2 NS-1; (b) NCCNF@MnO_2 NS-2; (c) NCCNF@MnO_2 NS-3; (d) NCCNF@MnO_2 NS-4; (e) NCCNF@MnO_2 NS-5; and (f) the corresponding digital photo of highly flexible NCCNF@MnO_2 NS-3 hybrid membrane.

effectively prevent the aggregation of MnO_2 nanoparticles (Figure S1, Supporting Information), as well as provide an open 3D structure to enhance electron transfer during the charge−discharge processes.

In order to reveal the simplicity and universality of this method, a "mace-like" hybrid nanostructure was obtained by replacing $KMnO_4$ with $Mn(SO_4)_2$ and $(NH_4)_2S_2O_8$ as precursors for the redox reactions. MnO_2 nanorods with diameter of 20−50 nm were perpendicularly and densely grown on the surface of NCCNF as shown in Figure 4a and 4b. This hierarchical core−sheath nanostructure can also effectively prevent the aggregation of MnO_2 nanoparticles (Figure S2, Supporting Information), which can largely improve the specific surface area of MnO_2 as well as increase the penetration of electrolyte during the electrochemical processes. The crystal structures of MnO_2 nanosheets and nanorods were verified by using XRD, as shown in Figure 5. For the bare CNF membrane, a very weak diffraction peak at 2θ = 25.1° can be hardly observed (detailed information can be seen in Figure S3, Supporting Information), indicating its poor crystallinity. Four distinct diffraction peaks located at 2θ = 19.3°, 37.2°, 43.9°, and 63.2° in the XRD pattern of the NCCNF membrane can be indexed to (111), (331), (400), and (440) reflections of cubic $NiCo_2O_4$ (JCPDS No. 20-0781), indicating the successful hybridization of $NiCo_2O_4$ particles into carbon nanofibers.[40] The XRD pattern of the NCCNF@MnO_2 NS membrane shows three diffraction peaks at 2θ = 12.7°, 26.3°, and 37.2°, which can be ascribed to the characteristic (001), (002), and (111) peaks of birnessite-type MnO_2 (JCPDS No. 80-1098).[41] Birnessite-type MnO_2 (also denoted as δ-MnO_2) has a two-dimensional lamellar structure with an interlayer distance of 0.73 nm, which is beneficial to the storage of electrolyte between the layer-by-layer structures, thus contributing to the

DOI: 10.1021/acs.jpcc.5b02739
J. Phys. Chem. C 2015, 119, 13442−13450

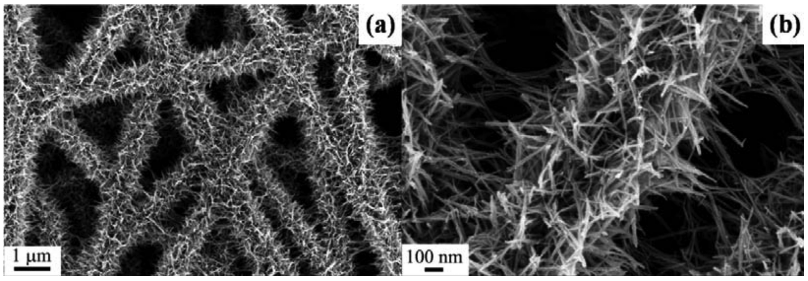

Figure 4. FESEM images of the NCCNF@MnO_2 NR with different magnifications.

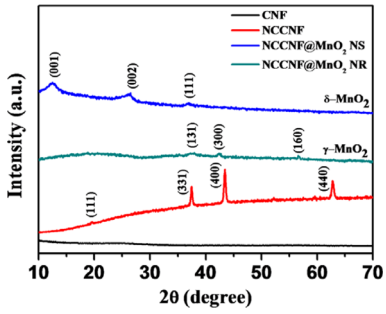

Figure 5. XRD patterns of the bare electrospun CNF membrane, $NiCo_2O_4$-doped CNF, $NiCo_2O_4$-doped CNF@MnO_2 nanosheet, and $NiCo_2O_4$-doped CNF@MnO_2 nanorod membranes.

intimate contact between OH^- and MnO_2 nanosheets. Similarly, the weak peaks located at 2θ = 37.6°, 42.4°, and 56.7° of the NCCNF@MnO_2 NR membrane are indexed to (131), (300), and (160) reflections of the γ-phase crystal form of MnO_2 nanorods, respectively.[42] The γ-phase of MnO_2 is generated by its "De Wolff" structural disorder as reported previously,[43] the high crystallinity of which is beneficial to nonaqueous electrochemical applications.[44]

The compositions and chemical states of NCCNF@MnO_2 NS and NCCNF@MnO_2 NR hybrid membranes were analyzed by XPS spectra as shown in Figure 6. Mn, C, and O can be

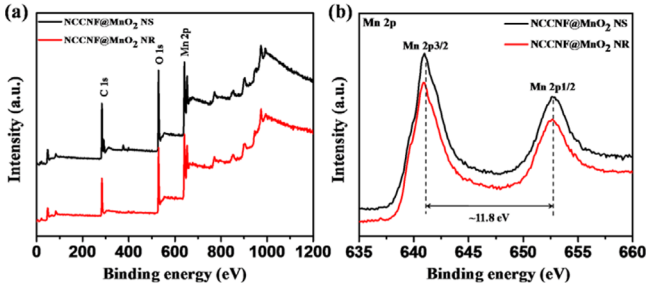

Figure 6. XPS spectra of the NCCNF@MnO_2 nanosheet and nanorod hybrid membranes: (a) the full survey scan and (b) high-resolution scans for Mn 2p.

clearly identified for both NCCNF@MnO_2 NS and NCCNF@MnO_2 NR hybrid membranes from the survey spectra in Figure 6a. Meanwhile, the binding energies of Mn $2p_{3/2}$ and Mn $2p_{1/2}$ are, respectively, centered at 640.9 and 652.7 eV in Mn 2p spectra with a spin energy difference of ~11.8 eV (Figure 6b), which matches well with a previous report,[45] thus not only providing direct evidence for the presence of the MnO_2 phase but also indicating the same oxidation state of manganese in both NCCNF@MnO_2 NS and NCCNF@MnO_2 NR hybrid membranes. Furthermore, TGA curves (Figure S4, Supporting Information) were collected to demonstrate the respective weight (Table S1, Supporting Information) of $NiCo_2O_4$ nanoparticles and MnO_2 NS or NR for the subsequent electrochemical calculations.

The electrochemical performances were evaluated in a three-electrode system for supercapacitors. Cyclic voltammetry (CV) curves in Figure 7a indicate that the NCCNF@MnO_2 NS-3 hybrid membrane possesses a significantly higher specific capacitance than the bare CNF, NCCNF, and CNF@MnO_2 NS-1:1 membranes, which can be attributed to the synergistic interactions between the highly conductive NCCNF template and uniformly distributed MnO_2 nanosheets. First, hybridization of $NiCo_2O_4$ nanoparticles into CNF can achieve a synergistic enhancement in their capacitance due to high conductivity of NCCNF and pseudocapacitive characteristics of $NiCo_2O_4$ nanoparticles. Second, electrochemical properties can be significantly improved due to the pseudocapacitive characteristics of MnO_2 nanosheets and their uniform growth on the surface of nanofibers. CV curves of NCCNF@MnO_2 NS membrane electrodes with different weight ratios of the NCCNF membrane to $KMnO_4$ were collected at a scan rate of 100 mV s^{-1} (Figure 7b), which exhibit quasi-rectangles and mirror-image symmetry, thus demonstrating their ideal capacitive behavior. The NCCNF@MnO_2 NS-3 membrane electrode exhibits the optimal specific capacitance of 501 F g^{-1} (based on the active materials) at 100 mV s^{-1} among these five samples. Moreover, the excessive consumption of the carbon backbone (for the cases of NCCNF@MnO_2 NS-4 and NCCNF@MnO_2 NS-5) with luxuriant growth of MnO_2 nanosheets dramatically hinders electrolyte penetration and electron transport during electrochemical processes, thus resulting in negative effects on the final electrochemical performance. Due to the excellent conductivity and optimal MnO_2 content in the NCCNF@MnO_2 NS-3 hybrid membrane, rectangular shapes of the CV curves at scan rates from 2 to 100 mV s^{-1} are retained in Figure 7c. The high specific capacitance of 309 F g^{-1} based on the whole electrode, that is, 918 F g^{-1} based on the active materials, is achieved for the NCCNF@MnO_2 NS-3 hybrid membrane at a scan rate of 2 mV s^{-1}, much higher than the previously reported value (530 F g^{-1} at a scan rate of 2 mV s^{-1}) for the coaxial carbon nanofiber/MnO_2 nanocomposite approaching the theoretical value of MnO_2.[34] Furthermore, the linear and symmetrical galvanostatic charge−discharge curves (Figure 7d) of the NCCNF@MnO_2 NS-3 membrane electrode manifest its rapid voltage−current response and excellent electrochemical reversibility. Even high rate retention of 248 F g^{-1} is achieved at 10 A g^{-1} for the NCCNF@MnO_2 NS-3 hybrid membrane, indicating high rate capability as electrode materials. As shown in Figure 7e, CNF and NCCNF membranes exhibit extremely excellent rate stabilities but low specific capacitances. With increasing the

DOI: 10.1021/acs.jpcc.5b02739
J. Phys. Chem. C 2015, 119, 13442−13450

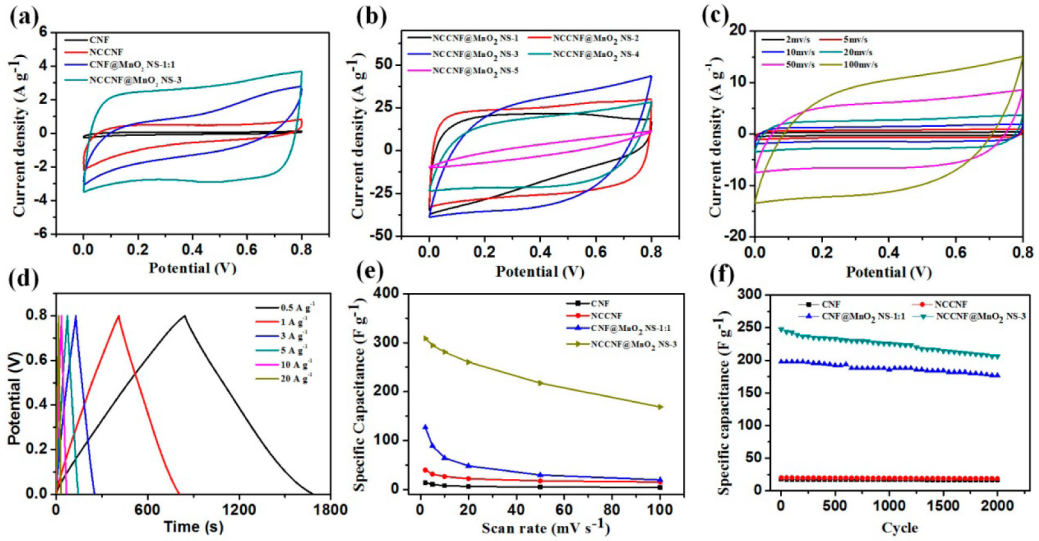

Figure 7. (a) CV curves of bare CNF, NCCNF, CNF@MnO_2 NS-1:1, and NCCNF@MnO_2 NS-3 membranes at a scan rate of 20 mV·s^{-1}. (b) CV curves of the NCCNF@MnO_2 nanosheet (based on the active materials) at a scan rate of 100 mV·s^{-1}. (c) CV curves of the NCCNF@MnO_2 NS-3 hybrid membrane at different scan rates. (d) Galvanostatic charge−discharge curves with different current densities for the NCCNF@MnO_2 nanosheet electrode. (e) Rate stability of bare CNF, NCCNF, CNF@MnO_2 NS-1:1, and NCCNF@MnO_2 NS-3 membranes at different scan rates. (f) Cycling stability of different samples at a current density of 10 A g^{-1}.

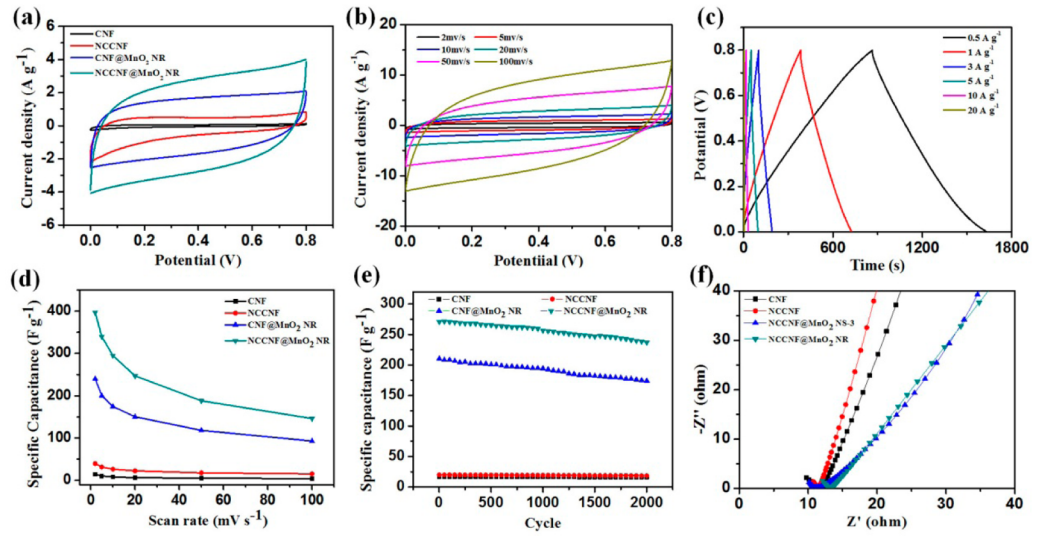

Figure 8. (a) CV curves of bare CNF, NCCNF, CNF@MnO_2 NR, and NCCNF@MnO_2 NR membranes at a scan rate of 20 mV·s^{-1}. (b) CV curves of the NCCNF@MnO_2 NR membrane at different scan rates. (c) Galvanostatic charge−discharge curves with different current densities for the NCCNF@MnO_2 nanorod electrode. (d) Rate stability of bare CNF, NCCNF, CNF@MnO_2 nanorod, and NCCNF@MnO_2 nanorod membranes at different scan rates. (e) Cycling stability of different samples at 10 A g^{-1}. (f) Nyquist plots of bare CNF, NCCNF, NCCNF@MnO_2 nanosheet, and nanorod membranes obtained at open-circuit potentials.

coating of MnO_2 sheath, the rate stability shows a slight decrease due to excess consumption of the carbon backbone which is the key contributor for the high rate stability of the as-obtained hybrid electrode materials (Figure S5, Supporting Information). Therefore, the NCCNF@MnO_2 NS-3 hybrid membrane shows the highest specific capacitance as well as acceptable rate stability for supercapacitor applications. As shown in Figure 7f, cycling life tests for bare CNF, NCCNF, CNF@MnO_2 NS-1:1, and NCCNF@MnO_2 NS-3 membranes were carried out at 10 A g^{-1} for over 2000 cycles. The NCCNF@MnO_2 NS-3 electrode exhibits a high retention of 83.3%, which is also evident from the stable charge−discharge curves of the last 20 cycles (Figure S6a, Supporting Information) with almost 99% Coulombic efficiency.

Quasi-rectangular and mirror-image symmetrical CV curves can also be observed for the "mace-like" nanostructured NCCNF@MnO_2 NR hybrid membrane, as shown in Figure 8a and 8b. The NCCNF@MnO_2 NR hybrid membrane exhibits higher specific capacitance of 308 F g^{-1} (based on the whole electrode) at a scan rate of 2 mV s^{-1}, i.e., 827 F g^{-1} (based on the active materials), over bare CNF, NCCNF, or CNF@MnO_2 NR membranes. Linear and symmetrical galvanostatic charge−discharge curves of the NCCNF@MnO_2 NR electrode at different current densities are shown in Figure 8c, exhibiting a high specific capacitance of 477 F g^{-1}

DOI: 10.1021/acs.jpcc.5b02739
J. Phys. Chem. C 2015, 119, 13442−13450

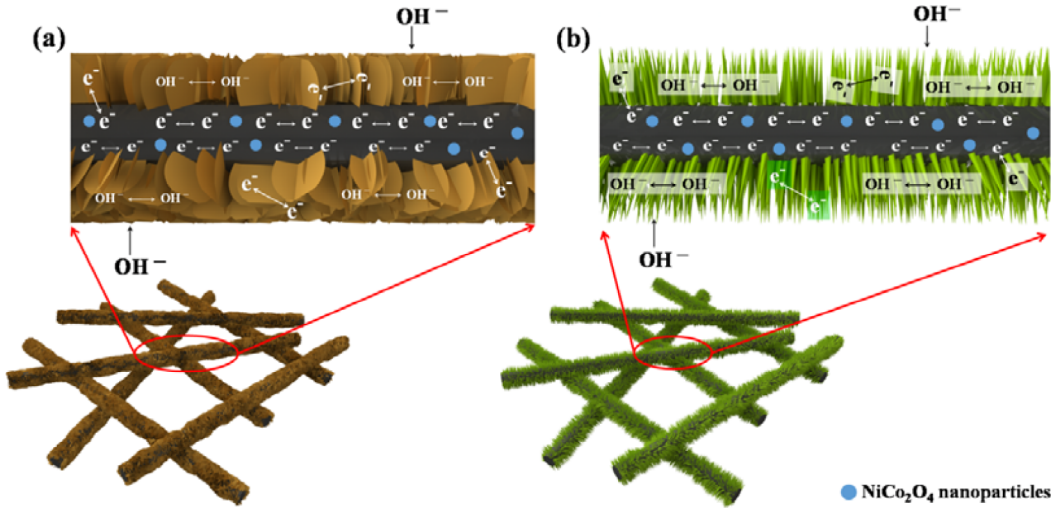

Figure 9. Illustration of the electron and ion transport pathways in the (a) NCCNF@MnO_2 NS hybrid membrane and (b) NCCNF@MnO_2 NR hybrid membrane.

at a current density of 0.5 A g^{-1}. The scan rate dependence of the specific capacitance (Figure 8d) reveals an excellent rate stability with high specific capacitance of 146 F g^{-1} (based on whole materials) at a scan rate of 100 mV s^{-1} for the NCCNF@MnO_2 NR hybrid membrane. The cycling stability of the NCCNF@MnO_2 NR electrode is shown in Figure 8e with a high retention of 87.6% even after 2000 cycles, which is comparable with the stable performance of bare CNF and NCCNF membranes. Furthermore, the charge−discharge curves of the last 20 cycles indicate a high Coulombic efficiency for the NCCNF@MnO_2 NR hybrid membrane as shown in Figure S6b (Supporting Information). Thus, it proves an easy and versatile approach via the combination of electrospinning and redox deposition processes to prepare three-dimensional and flexible carbon nanofiber@MnO_2 hybrid electrode materials with different morphologies and crystal forms of MnO_2 nanoparticles.

As mentioned above, the specific capacitance of the NCCNF@MnO_2 NS-3 hybrid membrane is 918 F g^{-1} (based on the active materials) at a scan rate of 2 mV s^{-1}, which is higher than that (827 F g^{-1}) of the NCCNF@MnO_2 NR hybrid membrane. This can be attributed to the different crystal forms of MnO_2 in these two hybrid membranes. As reported previously, the electrochemical performance of MnO_2 is closely related to its crystal forms, which decreases by the following order: $\alpha \approx \delta > \gamma > \lambda > \beta$.[46,47] The layer-by-layer structure of δ-MnO_2 is beneficial to the penetration of electrolyte due to its high content of crystal water. However, γ-type MnO_2 is relatively regular with a low content of crystal water, which severely limits ion exchange during the charge−discharge processes. Therefore, the ultimate electrochemical performance of the NCCNF@MnO_2 NS hybrid membrane is better than that of the NCCNF@MnO_2 NS hybrid membrane.

EIS was measured to investigate the electrochemical impedance of bare CNF, NCCNF, NCCNF@MnO_2 NS-3, and NCCNF@MnO_2 NR membranes in the frequency range of 100 kHz to 0.01 Hz, as shown in Figure 8f. All plots display a part of the semicircle at a high-frequency region and a straight line in the low-frequency region, which, respectively, correspond to the electron-transfer processes and diffusion processes. The smaller semicircle in the high-frequency region and steeper slope in the low-frequency region for the NCCNF membrane over the CNF membrane (Figure S7, Supporting Information) indicate an enhanced conductivity due to the hybridization of $NiCo_2O_4$ nanoparticles into carbon nanofibers. Furthermore, low electrode−electrolyte interfacial resistances for both NCCNF@MnO_2 NS and NCCNF@MnO_2 NR hybrid membranes also indicate remarkably excellent electrolyte penetration of these two electrode materials.

The excellent performance of MnO_2 NS and NR on CNF membranes can be attributed to the following aspects: (1) The uniform and immense growth of MnO_2 nanosheets and nanorods on the surface of $NiCo_2O_4$-doped carbon nanofibers effectively prevents the aggregation of MnO_2 nanoparticles, which obviously increases its specific surface area as well as provides more active sites for ionic adsorption. (2) Carbon nanofibers, as typical electrical double-layer capacitor materials, possess high electrical conductivity, which contribute to faster electron transportation during the electrochemical processes. (3) Uniformly distributed $NiCo_2O_4$ nanoparticles in CNF can not only increase the conductivity of CNF membranes but also act as numerous energy-storage units to enhance the pseudocapacitive performance. (4) The nonwoven electrospun membrane provides an enormous and open three-dimensional network, which facilitates the penetration of electrolytes and transport of electrons as illustrated in Figure 9. Therefore, this new kind of flexible hybrid membrane with hierarchical nanostructures obtained by direct redox deposition of pseudocapacitive MnO_2 nanoparticles on highly conductive electrospun carbon nanofibers offers great promise as binder-free electrodes for high-performance energy storage devices.

4. CONCLUSIONS

In summary, $NiCo_2O_4$-doped carbon nanofiber@MnO_2 nanosheet and nanorod hybrid membranes with different crystal forms of MnO_2 nanostructures were facilely synthesized by combining electrospinning, solution codeposition, and redox deposition methods. Birnessite-type MnO_2 nanosheets and γ-phase MnO_2 nanorods are uniformly and densely anchored on the surface of $NiCo_2O_4$-doped carbon nanofibers to form an open three-dimensional network, which can efficiently increase the specific surface areas for ionic adsorption and offers intersecting pathways for electron transport during the charge−discharge processes. Thus, remarkably enhanced specific

DOI: 10.1021/acs.jpcc.5b02739
J. Phys. Chem. C 2015, 119, 13442−13450

capacitances of 918 and 827 F g^{-1} (based on the active materials) at a scan rate of 2 mV s^{-1} are, respectively, achieved for NCCNF@MnO_2 NS and NCCNF@MnO_2 NR hybrid membranes, with excellent rate and cycling stabilities. Our results imply that $NiCo_2O_4$-doped CNF@MnO_2 nanosheet and nanorod hybrid membranes are promising electroactive materials for high-performance supercapacitors.

■ ASSOCIATED CONTENT

Supporting Information

Figure S1 shows FESEM images of bare MnO_2 nanosheets without $NiCo_2O_4$-doped carbon nanofibers as template at different magnifications. Figure S2 shows FESEM images of bare MnO_2 nanorods without $NiCo_2O_4$-doped carbon nanofibers as template at different magnifications. Figure S3 presents a detailed XRD pattern of the bare electrospun CNF membrane. Figure S4 displays TGA profiles of bare CNF, NCCNF, NCCNF@MnO_2 NS-1, NCCNF@MnO_2 NS-2, NCCNF@MnO_2 NS-3, NCCNF@MnO_2 NS-4, NCCNF@MnO_2 NS-5, and NCCNF@MnO_2 NR membranes obtained under air flow at a temperature ramp of 10 °C min^{-1}. Figure S5 shows rate stability of NCCNF@MnO_2 nanosheet hybrid membranes at different scan rates. Figure S6 presents the charge−discharge curves of the last 20 cycles for (a) NCCNF@MnO_2 NS-3 hybrid membrane and (b) NCCNF@MnO_2 NR hybrid membrane. Figure S7 shows the magnified Nyquist plots of bare CNF and NCCNF membranes. The Supporting Information is available free of charge on the ACS Publications website at DOI: 10.1021/acs.jpcc.5b02739.

■ AUTHOR INFORMATION

Corresponding Author

*E-mail: txliu@fudan.edu.cn. Tel.: +86-21-55664197. Fax: +86-21-65640293.

Notes

The authors declare no competing financial interest.

■ ACKNOWLEDGMENTS

The authors are grateful for the financial support from the National Natural Science Foundation of China (51125011, 51373037, 51433001).

■ REFERENCES

(1) Tarascon, J. M.; Armand, M. Issues and Challenges Facing Rechargeable Lithium Batteries. *Nature* **2001**, *414*, 359−367.

(2) Guo, Y.; Hu, J.; Wan, L. Nanostructured Materials for Electrochemical Energy Conversion and Storage Devices. *Adv. Mater.* **2008**, *20*, 2878−2887.

(3) Yang, Z.; Zhang, J.; Kintner-Meyer, M. C. W.; Lu, X.; Choi, D.; Lemmon, J. P.; Liu, J. Electrochemical Energy Storage for Green Grid. *Chem. Rev.* **2011**, *111*, 3577−3613.

(4) Liu, M. K.; Tjiu, W. W.; Pan, J. S.; Zhang, C.; Gao, W.; Liu, T. X. One-Step Synthesis of Graphene Nanoribbon-MnO_2 Hybrids and Their All-Solid-State Asymmetric Supercapacitors. *Nanoscale* **2014**, *6*, 4233−4242.

(5) Han, L.; Tang, P.; Zhang, L. Hierarchical Co_3O_4@PPy@MnO_2 Core-Shell-Shell Nanowire Arrays for Enhanced Electrochemical Energy Storage. *Nano Energy* **2014**, *7*, 42−51.

(6) Xu, K.; Li, W.; Liu, Q.; Li, B.; Liu, X.; An, L.; Chen, Z.; Zou, R.; Hu, J. Hierarchical Mesoporous $NiCo_2O_4$@MnO_2 Core-Shell Nanowire Arrays on Nickel Foam for Aqueous Asymmetric Supercapacitors. *J. Mater. Chem. A* **2014**, *2*, 4795−4802.

(7) Zhang, Y. F.; Fan, W.; Huang, Y. P.; Zhang, C.; Liu, T. X. Graphene/Carbon Aerogels Derived from Graphene Crosslinked Polyimide as Electrode Materials for Supercapacitors. *RSC Adv.* **2015**, *5*, 1301−1308.

(8) Wang, H.; Hao, Q.; Yang, X.; Lu, L.; Wang, X. A Nanostructured Graphene/Polyaniline Hybrid Material for Supercapacitors. *Nanoscale* **2010**, *2*, 2164−2170.

(9) Hu, C.; Chang, K.; Lin, M.; Wu, Y. Design and Tailoring of the Nanotubular Arrayed Architecture of Hydrous RuO_2 for Next Generation Supercapacitors. *Nano Lett.* **2006**, *6*, 2690−2695.

(10) Hyun, T.; Kang, J.; Kim, H.; Hong, J.; Kim, I. Electrochemical Properties of MnO_x-RuO_2 Nanofiber Mats Synthesized by Co-Electrospinning. *Electrochem. Solid State Lett.* **2009**, *12*, A225−A228.

(11) Wang, G.; Zhang, L.; Zhang, J. A Review of Electrode Materials for Electrochemical Supercapacitors. *Chem. Soc. Rev.* **2012**, *41*, 797−828.

(12) Wei, W.; Cui, X.; Chen, W.; Ivey, D. G. Manganese Oxide-Based Materials as Electrochemical Supercapacitor Electrodes. *Chem. Soc. Rev.* **2011**, *40*, 1697−1721.

(13) Chen, Z.; Jiao, Z.; Pan, D.; Li, Z.; Wu, M.; Shek, C.; Wu, C. M. L.; Lai, J. K. L. Recent Advances in Manganese Oxide Nanocrystals: Fabrication, Characterization, and Microstructure. *Chem. Rev.* **2012**, *112*, 3833−3855.

(14) Liu, J.; Jiang, J.; Cheng, C.; Li, H.; Zhang, J.; Gong, H.; Fan, H. J. Co_3O_4 Nanowire@MnO_2 Ultrathin Nanosheet Core/Shell Arrays: A New Class of High-Performance Pseudocapacitive Materials. *Adv. Mater.* **2011**, *23*, 2076.

(15) Subramanian, V.; Zhu, H. W.; Vajtai, R.; Ajayan, P. M.; Wei, B. Q. Hydrothermal Synthesis and Pseudocapacitance Properties of MnO_2 Nanostructures. *J. Phys. Chem. B* **2005**, *109*, 20207−20214.

(16) Nayak, P. K.; Munichandraiah, N. Rapid Sonochemical Synthesis of Mesoporous MnO_2 for Supercapacitor Applications. *Mater. Sci. Eng. B: Adv. Funct. Solid-State Mater.* **2012**, *177*, 849−854.

(17) Zhang, X.; Sun, X.; Zhang, H.; Zhang, D.; Ma, Y. Development of Redox Deposition of Birnessite-type MnO_2 on Activated Carbon as High-Performance Electrode for Hybrid Supercapacitors. *Mater. Chem. Phys.* **2012**, *137*, 290−296.

(18) Zang, J.; Li, X. In Situ Synthesis of Ultrafine beta-MnO_2/Polypyrrole Nanorod Composites for High-Performance Supercapacitors. *J. Mater. Chem.* **2011**, *21*, 10965−10969.

(19) Toupin, M.; Brousse, T.; Belanger, D. Charge Storage Mechanism of MnO_2 Electrode Used in Aqueous Electrochemical Capacitor. *Chem. Mater.* **2004**, *16*, 3184−3190.

(20) Sassin, M. B.; Hoag, C. P.; Willis, B. T.; Kucko, N. W.; Rolison, D. R.; Long, J. W. Designing High-Performance Electrochemical Energy-Storage Nanoarchitectures to Balance Rate and Capacity. *Nanoscale* **2013**, *5*, 1649−1657.

(21) Tang, W.; Hou, Y. Y.; Wang, X. J.; Bai, Y.; Zhu, Y. S.; Sun, H.; Yue, Y. B.; Wu, Y. P.; Zhu, K.; Holze, R. A Hybrid of MnO_2 Nanowires and MWCNTs as Cathode of Excellent Rate Capability for Supercapacitors. *J. Power Sources* **2012**, *197*, 330−333.

(22) Yuan, L.; Lu, X.; Xiao, X.; Zhai, T.; Dai, J.; Zhang, F.; Hu, B.; Wang, X.; Gong, L.; Chen, J.; Hu, C.; Tong, Y.; Zhou, J.; Wang, Z. L. Flexible Solid-State Supercapacitors Based on Carbon Nanoparticles/MnO_2 Nanorods Hybrid Structure. *ACS Nano* **2012**, *6*, 656−661.

(23) Chen, L.; Huang, Z.; Liang, H.; Guan, Q.; Yu, S. Bacterial-Cellulose-Derived Carbon Nanofiber@MnO_2 and Nitrogen-Doped Carbon Nanofiber Electrode Materials: An Asymmetric Supercapacitor with High Energy and Power Density. *Adv. Mater.* **2013**, *25*, 4746−4752.

(24) Fan, Z.; Yan, J.; Wei, T.; Zhi, L.; Ning, G.; Li, T.; Wei, F. Asymmetric Supercapacitors Based on Graphene/MnO_2 and Activated Carbon Nanofiber Electrodes with High Power and Energy Density. *Adv. Funct. Mater.* **2011**, *21*, 2366−2375.

(25) Ren, Y. M.; Xu, Q.; Zhang, J. M.; Yang, H. X.; Wang, B.; Yang, D. Y.; Hua, J. H.; Liu, Z. M. Functionalization of Biomass Carbonaceous Aerogels: Selective Preparation of MnO_2@CA Composites for Supercapacitors. *ACS Appl. Mater. Interfaces* **2014**, *6* (12), 9689−9697.

(26) You, B.; Li, N.; Zhu, H.; Zhu, X.; Yang, J. Graphene Oxide-Dispersed Pristine CNTs Support for MnO_2 Nanorods as High

Performance Supercapacitor Electrodes. *ChemSusChem* **2013**, *6*, 474−480.
(27) Zhao, Y.; Meng, Y.; Jiang, P. Carbon@MnO_2 Core-Shell Nanospheres for Flexible High-Performance Supercapacitor Electrode Materials. *J. Power Sources* **2014**, *259*, 219−226.
(28) Seo, D. H.; Han, Z. J.; Kumar, S.; Ostrikov, K. K. Structure-Controlled, Vertical Graphene-Based, Binder-Free Electrodes from Plasma-Reformed Butter Enhance Supercapacitor Performance. *Adv. Energy Mater.* **2013**, *3*, 1316−1323.
(29) Yan, J. J.; Huang, Y. P.; Miao, Y. E.; Tjiu, W. W.; Liu, T. X. Polydopamine-Coated Electrospun Poly(Vinyl Alcohol)/Poly(Acrylic Acid) Membranes as Efficient Dye Adsorbent with Good Recyclability. *J. Hazard. Mater.* **2015**, *283*, 730−739.
(30) Cavaliere, S.; Subianto, S.; Savych, I.; Jones, D. J.; Roziere, J. Electrospinning: Designed Architectures for Energy Conversion and Storage Devices. *Energy Environ. Sci.* **2011**, *4*, 4761−4785.
(31) Zhang, P.; Shao, C.; Zhang, Z.; Zhang, M.; Mu, J.; Guo, Z.; Liu, Y. In Situ Assembly of Well-Dispersed Ag Nanoparticles (AgNPs) on Electrospun Carbon Nanofibers (CNFs) for Catalytic Reduction of 4-Nitrophenol. *Nanoscale* **2011**, *3*, 3357−3363.
(32) Kim, C.; Yang, K. S. Electrochemical Properties of Carbon Nanofiber Web as an Electrode for Supercapacitor Prepared by Electrospinning. *Appl. Phys. Lett.* **2003**, *83*, 1216−1218.
(33) Huang, Y. P.; Miao, Y. E.; Zhang, L. S.; Tjiu, W. W.; Pan, J. S.; Liu, T. X. Synthesis of Few-Layered MoS_2 Nanosheet-Coated Electrospun SnO_2 Nanotube Heterostructures for Enhanced Hydrogen Evolution Reaction. *Nanoscale* **2014**, *6*, 10673−10679.
(34) Wang, J.; Yang, Y.; Huang, Z.; Kang, F. Coaxial Carbon Nanofibers/MnO_2 Nanocomposites as Freestanding Electrodes for High-Performance Electrochemical Capacitors. *Electrochim. Acta* **2011**, *56*, 9240−9247.
(35) Zhi, M. J.; Manivannan, A.; Meng, F. K.; Wu, N. Q. Highly Conductive Electrospun Carbon Nanofiber/MnO_2 Coaxial Nano-Cables for High Energy and Power Density Supercapacitors. *J. Power Sources* **2012**, *208*, 345−353.
(36) Huang, Y. P.; Miao, Y. E.; Tjiu, W. W.; Liu, T. X. High-Performance Flexible Supercapacitors Based on Mesoporous Carbon Nanofibers/Co_3O_4/MnO_2 Hybrid Electrodes. *RSC Adv.* **2015**, *5*, 18952−18959.
(37) Jin, X.; Zhou, W.; Zhang, S.; Chen, G. Z. Nanoscale Microelectrochemical Cells on Carbon Nanotubes. *Small* **2007**, *3*, 1513−1517.
(38) Zhu, Z.; Qu, L.; Niu, Q.; Zeng, Y.; Sun, W.; Huang, X. Urchinlike MnO_2 Nanoparticles for the Direct Electrochemistry of Hemoglobin with Carbon Ionic Liquid Electrode. *Biosens. Bioelectron.* **2011**, *26*, 2119−2124.
(39) Chen, W.; Rakhi, R. B.; Wang, Q.; Hedhili, M. N.; Alshareef, H. N. Morphological and Electrochemical Cycling Effects in MnO_2 Nanostructures by 3D Electron Tomography. *Adv. Funct. Mater.* **2014**, *24*, 3130−3143.
(40) Yuan, C.; Li, J.; Hou, L.; Zhang, X.; Shen, L.; Lou, X. W. Ultrathin Mesoporous $NiCo_2O_4$ Nanosheets Supported on Ni Foam as Advanced Electrodes for Supercapacitors. *Adv. Funct. Mater.* **2012**, *22*, 4592−4597.
(41) Xiao, W.; Wang, D.; Lou, X. W. Shape-Controlled Synthesis of MnO_2 Nanostructures with Enhanced Electrocatalytic Activity for Oxygen Reduction. *J. Phys. Chem. C* **2010**, *114*, 1694−1700.
(42) Wang, X.; Li, Y. D. Synthesis and Formation Mechanism of Manganese Dioxide Nanowires/Nanorods. *Chem.—Eur. J.* **2003**, *9*, 300−306.
(43) Chabre, Y.; Pannetier, J. Structural and Electrochemical Properties of the Proton Gamma-MnO_2 System. *Prog. Solid State Chem.* **1995**, *23*, 1−130.
(44) Dose, W. M.; Sharma, N.; Webster, N. A. S.; Peterson, V. K.; Donne, S. W. Kinetics of the Thermally-Induced Structural Rearrangement of gamma-MnO_2. *J. Phys. Chem. C* **2014**, *118*, 24257−24265.
(45) Yan, J.; Fan, Z.; Wei, T.; Cheng, J.; Shao, B.; Wang, K.; Song, L.; Zhang, M. Carbon Nanotube/MnO_2 Composites Synthesized by Microwave-Assisted Method for Supercapacitors with High Power and Energy Densities. *J. Power Sources* **2009**, *194*, 1202−1207.
(46) Brousse, T.; Toupin, M.; Dugas, R.; Athouel, L.; Crosnier, O.; Belanger, D. Crystalline MnO_2 as Possible Alternatives to Amorphous Compounds in Electrochemical Supercapacitors. *J. Electrochem. Soc.* **2006**, *153*, A2171−A2180.
(47) Devaraj, S.; Munichandraiah, N. Effect of Crystallographic Structure of MnO_2 on Its Electrochemical Capacitance Properties. *J. Phys. Chem. C* **2008**, *112*, 4406−4417.

DOI: 10.1021/acs.jpcc.5b02739
J. Phys. Chem. C 2015, 119, 13442−13450